Catalysis Today 164 (2011) 251–256

Contents lists available at ScienceDirect

Catalysis Today

journal homepage: www.elsevier.com/locate/cattod

Preparation and characterization of CuO/ZnO–Al_2O_3 catalyst washcoats with CeO_2 sols for autothermal reforming of methanol in a microreactor

Kuen-Song Lin*, Sujan Chowdhury, Hsiu-Ping Yeh, Wang-Ting Hong, Chuin-Tih Yeh

Department of Chemical Engineering and Materials Science/Fuel Cell Center, Yuan Ze University, Chung-Li City 320, Taiwan, ROC

ARTICLE INFO

Article history:
Received 1 July 2010
Received in revised form
15 November 2010
Accepted 17 November 2010
Available online 30 December 2010

Keywords:
Washcoat
Microchannel
Ceria sol
Reforming
XANES/EXAFS
Fuel cell

ABSTRACT

Porous alumina support CuO/ZnO mixed with CeO_2 sols washcoat catalysts have been synthesized and characterized for the autothermal reforming of methanol in the present study. Experimentally, the BET N_2 adsorption for as-synthesized catalysts and catalyst mixtures with three different CeO_2 sols washcoats were 26, 31, 43, and 62 $m^2\ g^{-1}$, respectively. In addition, porosity of the catalyst is decreased significantly after certain amount of higher loading of the binder as confirmed using FE-SEM and BET measurements. The intensities of XRD and XPS data indicate that catalyst content copper species strongly interact with CeO_2 to from Cu–O–Ce. The EPR spectrum may reveal that Cu species may be mainly interacted with Ceria. The EXAFS data reveals that the Cu species have a Cu–O bonding with a bond distance of 1.99 ± 0.02 Å and coordination number is 3.24. Moreover, a hydrogen production rate of 2.16 L h^{-1} was obtained and the corresponding methanol conversion was 95% at 240 °C using the CuO/ZnO with 2 wt.% CeO_2 sol washcoat catalysts.

1. Introduction

Recently, primary fuel (such as methanol) oxidation through the catalysts is receiving considerable attention because of their potential role in the environmental friendly fuel cell technologies [1–3]. In the reported literatures, steam reforming of methanol (SRM) (Eq. (1)) and partial oxidation reaction of methanol (POM) (Eq. (2)) are consisted with production of hydrogen and are belonging with endothermic and exothermic reaction, respectively [3]. Combination of SRM and POM is effectively known as autothermal reforming (ATR) process and is attenuated with decreasing the reactor volume and design [3,4]. A SRM is the main reforming reaction provides the stoichiometric conversion of methanol to hydrogen. The SRM produces a relatively small amount of carbon monoxide at low temperatures; where as carbon monoxide is known to be very poisonous for Pt catalysts in a proton exchange membrane fuel cell (PEMFC) system [5]. In addition, autothermal reforming of methanol (ATRM) process leads to produce higher amount of hydrogen and consists with CO as a by-product which has negative impact on PEMFC operation. Therefore there is a great interest in developing highly selective catalysts.

$$CH_3OH(g) + H_2O(g) = CO_2 + 3H_2 \quad \Delta H^\circ = 49.5 \ \text{kJ mol}^{-1} \tag{1}$$

$$CH_3OH(g) + \tfrac{1}{2}O_2 = CO_2 + 2H_2 \quad \Delta H^\circ = -192.3 \ \text{kJ mol}^{-1} \tag{2}$$

The catalytic reaction for SRM and ATRM is generally based on copper or palladium. Where, Pd has consisted with higher thermal stability and the production of large content of CO with lower selectivity from methanol decomposition. On the other hand, Cu-based catalyst has consisted with low cost, higher reactivity, and selectivity [6,7]. In addition, copper catalyst is effectively dispersed in ZnO or ZnO/Al_2O_3 to generate mesoporosity, with high surface area and good thermal stability, exhibited interesting catalytic activity in the CO preferential oxidation reaction. Thus, CuO/ZnO–Al_2O_3 is one of the most used catalysts for hydrogen generation by ATRM and is coated on a microchannel reactor [1,2]. As well, cerium promoted copper catalyst is existed for the recovery of hydrogen from methanol with the optimization of carbonmonoxide concentration [8]. As an important component in catalysts, ceria promotes high oxygen storage capacity (OSC), oxygen vacancy, high oxygen ion conductivity and affective binder on microchannel reactor. Reduction of Ce(IV) to Ce(III) by oxygen ion leads to the generation of surface oxygen vacancy. These oxygen vacancies can act as promoting sites for the optimization of carbon monoxide concentration. Furthermore, ceria hindered Cu sintering in Cu/Al_2O_3 catalysts and increased thermal stability and catalytical reactivity [9]. According with the Germani et al. [2] binder plays a major role because of metal complexes formation

* Corresponding author at: Department of Chemical Engineering and Materials Science/Fuel Cell Center, Yuan Ze University, 135 Yuan-Tong Rd., Chung-Li City 320, Tao-Yuan County, Taiwan, ROC. Tel.: +886 34638800x2574; fax: +886 34559373.
E-mail address: kslin@saturn.yzu.edu.tw (K.-S. Lin).

0920-5861/$ – see front matter © 2010 Elsevier B.V. All rights reserved.
doi:10.1016/j.cattod.2010.11.038

is influenced the catalytic activities on the methanol decomposition reaction in the microchannel reactor. However, it is difficult to incorporate catalyst onto the microchannel reactor [2,10,11]. Several coating techniques have been applied for microchannels such as chemical vapor deposition, anodic oxidation, sol–gel process, washcoating, and electro-deposition to investigate the ATRM reaction [12–14]. The activities of catalysts are changed by the concentration differences for pre-sols and the treatment procedures of the drying and calcination temperatures [13]. Stutz and Poulikakos [14] indicate that a thinner catalyst layer is not sufficient to obtain higher catalyst activity in the ATRM reaction. In this present work, we were prepared $CuO/ZnO–Al_2O_3$ catalyst washcoats with CeO_2 sols and then to investigate the autothermal reforming of methanol in a microchannel reactor for a fuel cell system. In addition, the fine structures of catalyst washcoats were also identified and characterized using Brunauer–Emmer–Teller (BET) adsorption isotherms, field-emission scanning electron microscopy/energy dispersive X-ray spectroscopy (FE-SEM), X-ray powder diffraction (XRD), X-ray photoelectron spectroscopy (XPS), electron paramagnetic resonance (EPR), X-ray absorption near edge structure (XANES), and extended X-ray absorption fine structure (EXAFS) techniques.

2. Experimental

Microchannels in this microreactor were made of stainless steel SUS 304 by an etching process and included with a flow route of reactants and products. The size of the plate with microchannel was 60 (L) mm × 35 (W) mm × 0.6 (T) mm. The plate was designed with thirty-four microchannels with the plate of 35 (L) mm × 0.4 (W) mm × 0.2 (D) mm. CH_3OH and O_2 or water mixtures were passed through the right or left upper inlet and were distributed over the plates sequentially to the parallel microchannels. Finally, H_2/CO_2 mixtures were collected through the outlet at the bottom side. A graphite gasket was used between microchannel plates for gastight and the whole reactor was contained in stainless-steel housing.

As-synthesized homogeneous sol was prepared by adding 20 g as-synthesized catalyst (CuO 40%, ZnO 50%, and Al_2O_3 10%) and reosmosis water (ROM) (catalyst:ROM = 1:2) with a magnetic stirrer for continuous stirring at 500 rpm. Diluted homogeneous solution was prepared by dropwise addition of HNO_3 and NaOH to maintain the pH value at 9. The homogeneous solution was continuously stirred for 30 min to 6 h to obtain the catalyst slurry. After, stainless steel substrate surfaces were cleaned with acetone/$HNO_{3(aq)}$ and then the catalyst slurry (S20) was washcoated on the surface of microchannels with CeO_2 sol (as a binder (B) 1–10 wt.% of solid content, respectively), followed by drying at 25 °C for 5 h and then calcined at 350 °C for 2 h. The CeO_2 sol was used as a binder to enhance the adhesion between catalyst slurry and the SUS 304 or substrates. After calcinations CeO_2 film was formed between catalyst and substrate to obtain catalyst washcoat and denoted as S20-B1, S20-B2, and S20-B10, respectively.

The average concentrations of metals in washcoat catalysts were measured by inductively coupled plasma/mass spectroscopy (ICP/MS). The specific surface areas of as-synthesized $CuO/ZnO–Al_2O_3$ catalyst and the CeO_2 sols were measured according to the BET equation by nitrogen adsorption isotherms at 77 K (−196 °C) with a Micromeritics ASAP 2010 Instrument. For the BET surface area measurement, 0.2 g catalyst samples were ground, sieved, and filled into sample tubes. Prior to measurement, all catalyst samples were degassed at 423 K (150 °C) for 6 h. For the calculation of the BET surface areas, the relative pressure range P/P_0 of 0.05–0.2 was used. The pore radius distribution was determined using the method of Barrett, Joyner, and Halenda (BJH method). The morphologies, microstructures, and the elemental composition of the washcoat catalysts were determined by FE-SEM/EDS (JEOL 5600). Identification of the solid phases and crystalline structure of as-prepared catalyst sample was performed using XRD (Shimadzu Labx XRD-6000). All samples were therefore scanned from 20° to 80°(2θ) with a scan rate of 4°(2θ) min^{-1} and monochromatic CuK_α radiation. The recorded specific peak intensities and 2θ values can be further identified by a computer database system (JCPDS). Chemical structures of the fresh and washcoat catalysts were also measured by XPS (VG Scientific Fison ESCA 210) spectrometer at the excitation energy of MgK_α 1253.6 eV. Electron paramagnetic resonance (EPR) spectra were recorded on a Bruker ESP 300E (Bruker, Germany) spectrometer operating at X-band and equipped with a Bruker NMR gaussmeter ER 035 M and a Hewlett–Packard microwave frequency counter HP 5350B.

The XANES and EXAFS spectroscopies were collected at the Wiggler beamline 17C1 in the National Synchrotron Radiation Research Center (NSRRC) of Taiwan. The electron storage ring was operated with the energy of 1.5 GeV and a current of 100–200 mA. A Si(1 1 1) DCM was used for providing highly monochromatized photon beams with an energy of 4–15 keV (BL17C1) and resolving power ($E/\Delta E$) of up to 7000. Data were collected in fluorescence or transmission mode with a Lytle ionization detector [15] for Cu (8979 eV) K-edge experiments at room temperature. The photon energy was calibrated by characteristic preedge peaks in the absorption spectra of copper standards. Local structural parameters such as the bond distance (R), coordination number (CN), and Debye–Waller factor (σ) for different coordination shells surrounding the absorbing atoms were obtained through non-linear least-square fitting route. Moreover, the raw absorption data in the region of 50–200 eV below the edge position were also fit to a straight line using the least-square algorithms [15–17]. The XANES was extended to energy of the order of 50 eV above the edge. The k^2-weighted and EXAFS spectra were Fourier transformed to R space over the range between 2.5 and 12.5 $Å^{-1}$. The EXAFS data were analyzed using the UWXAFS 3.0 program and FEFF 8.2 codes [16,17].

The performance of methanol conversion tests was conducted in a lab-scale five-plate microchannel reactor using porous alumina support CuO/ZnO with CeO_2 sol catalysts washcoat. After the catalyst was applied in each plate then five plates were staked together with well sealed and integrated in a house. The total weight of as-synthesized catalyst coated on the five plates was 100 mg. A pre-mixture of methanol and water (1:1.3 molar ratio) solution was introduced to the microreactor using an automotive syringe pump with He carrier gas and then vaporized through a feed line heated at 182 °C. The feed rate of methanol liquid reactant mixtures was 0.05–0.2 mL min^{-1} with 16.2 g_{MeOH} h^{-1} $g_{cat.}{}^{-1}$ weight hourly space velocity in mass methanol per time and mass of catalyst (WHSV). The ATRM reaction was performed in the temperatures ranged of 210–300 °C. The microreactor was enclosed and heated by an electrically heated jacket and operated under isothermal with isobaric conditions including a temperature controller. Noncondensible gases stream of H_2, CO, and CO_2 generated in the microreactor were directly passed through an ice water cooler at 0 °C and were sampled or analyzed using a gas chromatography/thermal conductivity detector (GC/TCD) (Aligent 6890N). The conversion of methanol was calculated based on the methanol consumption as follows in the Eq. (3).

$$\text{Conversion}_{\text{MeOH}}(\%) = \frac{n_{\text{MeOH}_{\text{in}}} - n_{\text{MeOH}_{\text{out}}}}{n_{\text{MeOH}_{\text{in}}}} \times 100\% \quad (3)$$

where $n_{\text{MeOH}_{\text{in}}}$ and $n_{\text{MeOH}_{\text{out}}}$ were the molar flow rate of methanol. Subscripts in and out denote the inlet and outlet molar flow rates,

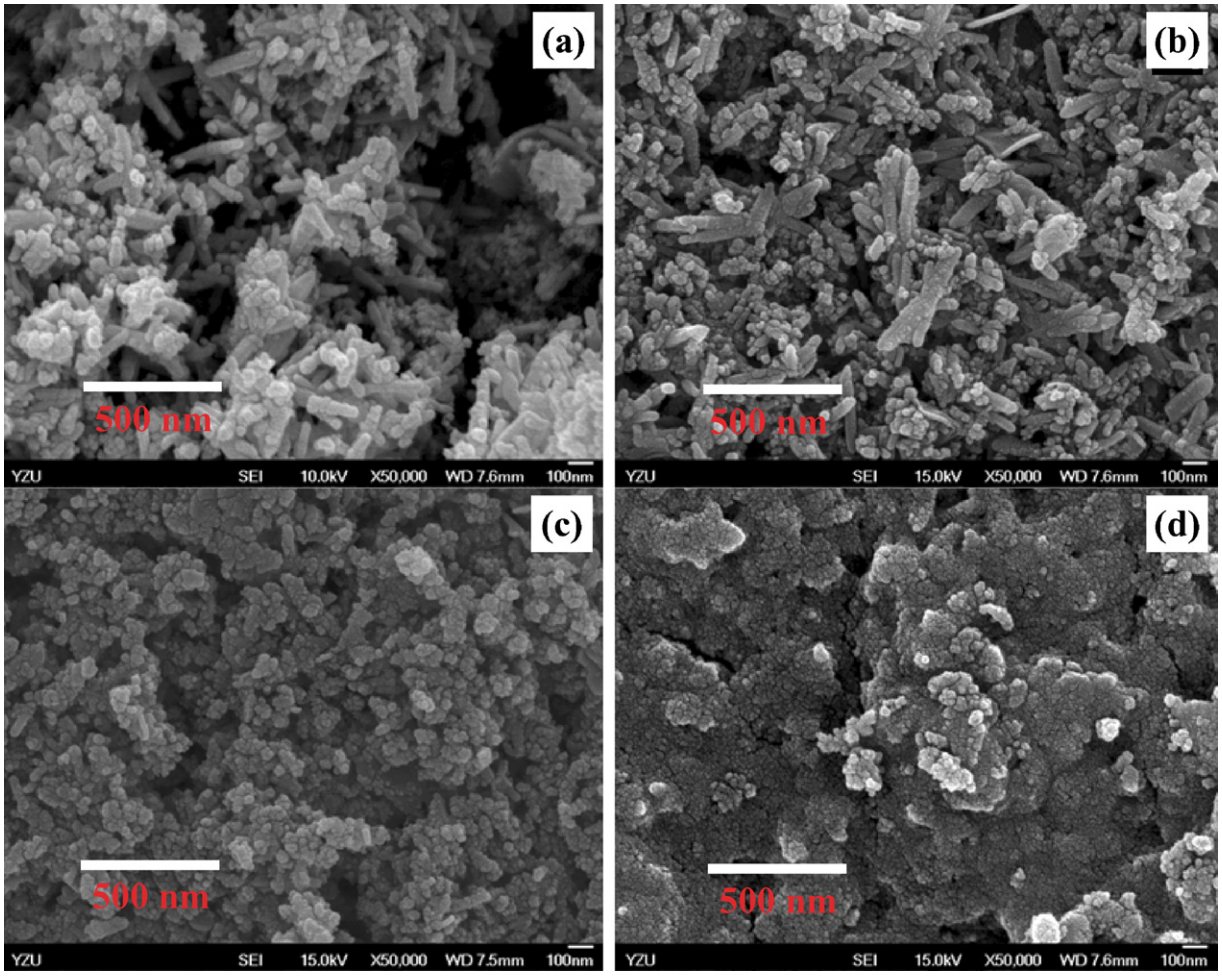

Fig. 1. FE-SEM microphotos of (a) CuO/ZnO–Al_2O_3 catalyst, catalyst washcoats of (b) S20-B1, (c) S20-B2, and (d) S20-B10, respectively.

respectively. The selectivity of CO was defined as follows in the Eq. (4)

$$\text{Selectivity}\,(\%) = \frac{n_{CO}}{n_{CO} + n_{CO_2}} \times 100\% \quad (4)$$

where n_{CO} and n_{CO_2} were represent the molar flow rate of CO and CO_2, respectively.

3. Results and discussion

According with the FE-SEM microphotos, the significant morphological differences between the as-prepared catalysts and the slurries are observed in Fig. 1. The irregular shapes of crystals in as-prepared catalysts and notably aggregated particles in CuO/ZnO–Al_2O_3 catalyst washcoats with CeO_2 sols were also found. In addition, as-synthesized catalyst has been gradually changed the color from deep brown into greenish blue after the addition of cerium sol solution and isopropyl alcohol (IPA). In fact, absorbance of water molecules shrink the electron density of Cu(II) ions. Therefore, it reveals that the copper species are associated with *d*–*d* transition state and Cu(II) ions coordination state is reflected the color changing behavior for washcoat slurry materials. Furthermore, BET N_2 adsorption for as-synthesized catalysts and catalytic mixtures with a CeO_2 sol washcoat were 26, 31, 43, and 62 $m^2\,g^{-1}$, respectively as shown in Table 1. It indicates that the addition of CeO_2 sols may promote to increase the surface area of the catalyst [18]. Moreover, porosity of the catalyst is decreased significantly after certain amount of higher loading of the binder as confirmed with the investigation of FE-SEM micrographs and BET measurements.

The X-ray diffraction patterns for the CuO/ZnO–Al_2O_3 catalyst and catalyst with CeO_2 binder washcoats are shown in Fig. 2. From Fig. 2(a), the weak peaks at Bragg angles 2θ of 43.3°, 50.14° and 74.1° for metallic copper (JCPDS 89-2838); 35.5° was attributed to CuO (JCPDS 89-5899) and also 36.52° and 73.7° was represented as Cu_2O (JCPDS 65-3288), respectively [8,9,18–20]. The characteristic peaks of ZnO were at 2θ of 31.80°, 34.51°, 36.30°, 62.82° and 69.10° (JCPDS 89-1397), respectively [18–20]. A peak of Al_2O_3 at 35.15°, 37.77°, 43.34°, 57.50°, 66.59°(JCPDS 82-1468) and spinal $CuAl_2O_4$ was also observed in the XRD spectra at 31.28°, 38.85° and 44.82°(JCPDS 78-0556), respectively [9]. While the characteristic weak peak of

Table 1
Specific surface area and average pore diameters of catalyst slurries.

Sample	Specific surface area ($m^2\,g^{-1}$)	Average pore diameter[a](nm)
CuO/ZnO–Al_2O_3	26.0	18.6
Slurry S20-B1[b]	31.0	30.0
Slurry S20-B2[c]	43.0	30.0
Slurry S20-B10[d]	62.0	10.0

[a] Average pore diameters were determined by BJH equation.
[b] Slurry of 20 wt.% solid content with 1 wt.% CeO_2 binder solid at pH 7.
[c] Slurry of 20 wt.% solid content with 2 wt.% CeO_2 binder solid at pH 7.
[d] Slurry of 20 wt.% solid content with 10 wt.% CeO_2 binder solid at pH 7.

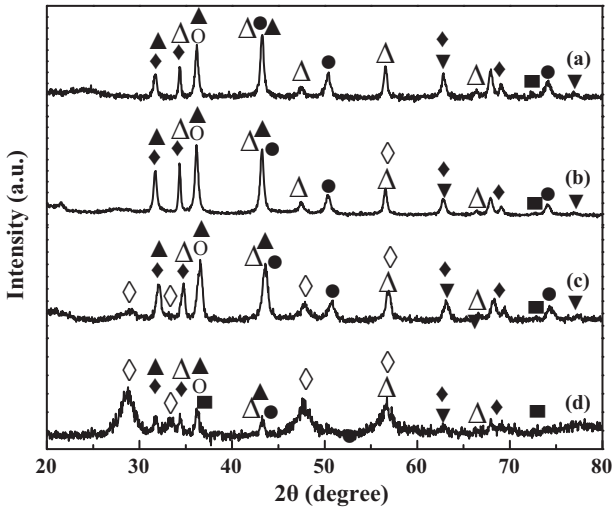

Fig. 2. XRD patterns of reduced (a) Cu/ZnO–Al_2O_3 catalyst, catalyst with CeO_2 binder washcoats of (b) S20-B1, (c) S20-B2, and (d) S20-B10, respectively (●: Cu; O: CuO; ■: Cu_2O; ♦: ZnO; ▲: $CuAl_2O_4$; ◊: CeO_2; △: Al_2O_3; ▼:SUS 304).

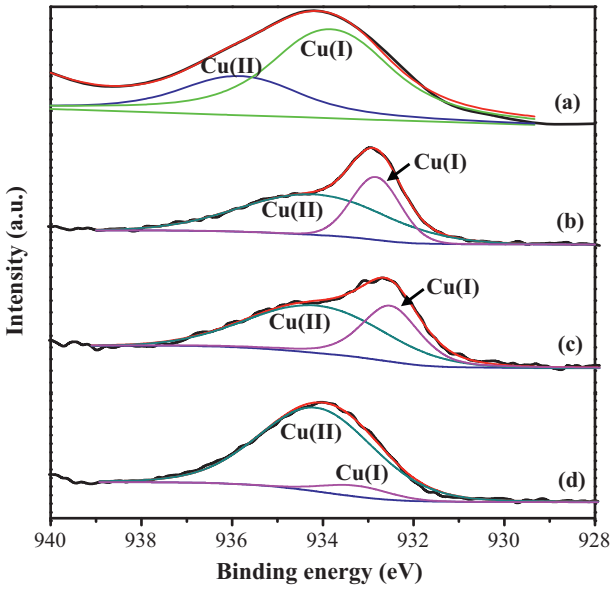

Fig. 3. X-ray photoelectron spectra of (a) a fresh Cu/ZnO–Al_2O_3 catalyst, catalyst with CeO_2 binder washcoats of (b) S20-B1, (c) S20-B2, and (d) S20-B10, respectively.

stainless steel at 2θ of 62.79° and 76.80° were attributed into Fig. 2. As shown in Fig. 2(b)–(d), XRD patterns of as-synthesized washcoat catalysts coated with increasing content of CeO_2 sols at 28.55°, 47.50° and 56.40° (JCPDS 81-0792) onto the surface of microreactor indicated that the Cu species were oxidized mainly into CuO [8,9]. Closer inspection of the XRD patterns revealed that the as synthesized washcoat catalyst has been consisted with the particle size around 18 nm and gradually decrease the size (as 13 ± 1 nm) with the increases of the loading of CeO_2 sols [9,18,19]. The peak width of copper for the increasing of CeO_2 loading is gradually affected to broaden than as synthesized sols and that represented the smaller copper particle sizes, as shown in Fig. 2(b)–(d). This suggested that CuO was finely dispersed on the surface of ceria or a Ce–O–Cu solid solution was formed [8,19]. Therefore, it was improved to facilitate the copper surface area and that is verified with the BET nitrogen adsorption isotherms analyses.

The catalysts represented in Fig. 3, are consisted with the higher concentration of aluminum rather than copper and zinc on the surface. Relative Cu:Ce surface concentration can be used to provide the information of amount Cu incorporation on to the catalyst washcoat. According with Fig. 3, the surface Cu to surface Ce atomic ratios are 0.60, 0.40, 0.07 for S20-B1, S20-B2, and S20-B10, respectively. It is suggested that increasing of ceria content take participate to disperse the copper species [19]. In addition, components observed (Fig. 3(b)–(d)) in catalyst washcoat at 934.5 eV were assigned to CuO. Most copper species are initially assisted as Cu(I) oxidation state and combined with ceria to form Cu–O–Ce species with the binding energy 932.8 eV [21,22]. Another Cu(II) species at 934.7 and 935.4 eV, respectively were related with consequent interaction of Cu(II) with aluminum to form $CuAl_2O_4$ or hydroxyl groups on ZnO surfaces [6,7,21–23]. A significant satellite peak of Cu(II) was also observed at 943 eV. Aluminum oxidation was significantly lowered in Fig. 3(c) due to the Ce species were combined with the Cu ones at higher temperatures and were formed Ce–O–Cu structures. This observation was similarly consistent and confirmed with the FE-SEM and XRD techniques. Since a washcoat provided a large surface area and porous structures, so that many active sites would be useful for the catalytic ATRM application.

The ATRM reaction was performed in order to investigate the as-synthesis catalyst activity in the stacked plate-typed reactor as revealed in Fig. 4 and Table 2. An ATRM performance was carried out at 210–300 °C with the same weight of coated catalysts packed in the microreactor. After the activation of the catalyst (S20-B2); methanol was started to decompose and the conversion was above 95% at 240 °C. In addition, a higher temperature was required for higher methanol conversion but decreasing with the increasing of feed flow rate and was related with the steam to carbon (methanol) ratio [24–26]. According with the Seo et al. [26], methanol conversion was achieved 90% at 260 °C and the feed flow rate was 0.2 $cm^3\,min^{-1}$. A hydrogen production rate of 2.16 $L\,h^{-1}$ was obtained at a feed rate of methanol liquid mixtures of 0.05–0.2 $mL\,min^{-1}$ with a WHSV of 16.2 $g_{MeOH}\,h^{-1}\,g_{cat.}{}^{-1}$. Moreover, the selectivity of hydrogen and carbon dioxide was high enough and a typical dry gas composition of the present system was 73–74% H_2, 24–25% CO_2, and <0.1% CO gas products, respectively. Nevertheless, a $T_r > 260 \pm 10$ °C was also required in the cases to achieve high methanol conversion [9–13,27]. The addition of ceria caused the synergistic effect to give the activity enhancement. However, methanol conversation was decreased to 95% at

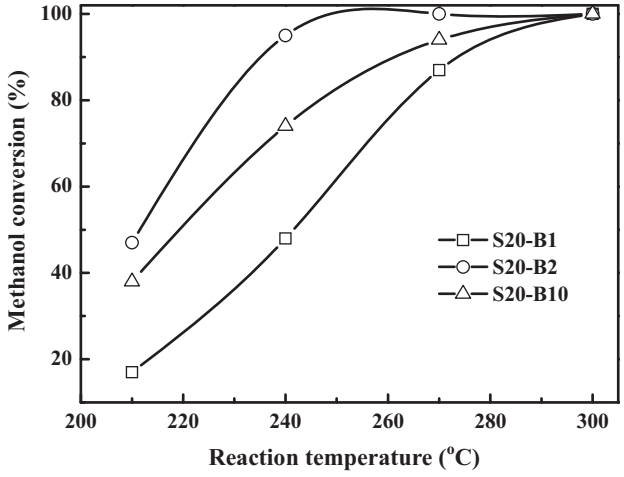

Fig. 4. Methanol conversion of Cu/ZnO–Al_2O_3 catalyst with CeO_2 binder washcoats of (a) S20-B1, (b) S20-B2, and (c) S20-B10, respectively for the steam reforming of methanol in a microreactor (steam/MeOH = 1.3; WHSV = 16.2 $g_{MeOH}\,h^{-1}\,g_{cat.}{}^{-1}$; loading weight of washcoat catalyst = 20 mg/plate).

Table 2
Comparison of the SRM/ATRM performances over different CuO/ZnO/CeO_2/ZrO_2/Al_2O_3 catalysts in the literatures.

Catalyst	S/C[a]	WHSV[b]	S_{CO} (%)	T_C[c] (°C)	Binder	Reference
$Cu_{40}Zn_{50}Al_{10}$	1.3	16.2	0.58	300 (95)	CeO_2	This work (S20-B1)
$Cu_{40}Zn_{50}Al_{10}$	1.3	16.2	0.40	240 (95)	CeO_2	This work (S20-B2)
$Cu_{40}Zn_{50}Al_{10}$	1.3	16.2	0.35	270 (95)	CeO_2	This work (S20-B10)
$Cu_{50}Zn_{33}Al_8$	1.1	54.0	2.90	260 (99)	Al_2O_3	Park et al. [11]
$Cu_{50}Zn_{33}Al_8$	1.5	14.8	1.10	270 (80)	ZrO_2	Lim et al. [13]
$Cu_{65}Zn_{28}Ce_7$	1.3	8.3	2.05	292 (97)	Al_2O_3	Yu et al. [9]
$Cu_{48}Zn_{48}Ce_4$	1.3	8.3	1.30	292 (98)	Al_2O_3	Yu et al. [9]
$Cu_{38}Zn_{58}Ce_4$	1.3	8.3	1.60	292 (91)	Al_2O_3	Yu et al. [9]
$Cu_{48}Zn_{48}Ce_4$	1.3	8.3	2.10	292 (88)	Al_2O_3	Yu et al. [9]
$Cu_{30}Zn_{60}Al_{10}$	1.1	14.1	0.47	250 (74)	N.A.	Huang et al. [27]
$Cu_{40}Zn_{50}Al_{10}$	1.1	14.1	0.49	250 (85)	N.A.	Huang et al. [27]
$Cu_{50}Zn_{40}Al_{10}$	1.1	14.1	0.50	300 (89)	N.A.	Huang et al. [27]
$Cu_{60}Zn_{30}Al_{10}$	1.1	14.1	0.49	300 (75)	N.A.	Huang et al. [27]

N.A. denotes "not available".
[a] S/C: steam to carbon ratio.
[b] WHSV: weight hourly space velocity in mass methanol per time and mass of catalyst ($g_{MeOH}\ h^{-1}\ g_{cat.}{}^{-1}$).
[c] (Temperature) (%) denotes "temperatures required for conversion of methanol at different percentage".

270 °C for S20-B10. Due to the morphology, porosity, BET surface area significantly affects the catalytic activity, the XRD patterns and XPS spectra were also confirmed [25–28]. This confirms that the as-synthesized catalyst are coated on to the microchannel reactor participates in an ATRM reaction and that is suitable for the integrated PEMFC application on energy generation.

Generally, Cu K-edge EXAFS spectroscopy can provide the information on the atomic arrangement of sorbents in terms of bond distance, coordination number, and kind of neighbors. A high reliability of the EXAFS data fitting for Cu species in as-synthesized and after reaction were obtained. Fourier transformation was performed on k^3-weighted oscillations over the range of 2.2 and 10 $Å^{-1}$. The XANES spectra of several different standards (Cu-foil, Cu_2O, and CuO) and the different samples of as-synthesized CuO/ZnO–Al_2O_3 catalysts with CeO_2 sols slurry and after reaction are shown in Fig. 5. The K-edge positions of standard Cu foil, Cu_2O, and CuO are 8978.2, 8979.36, and 8982.23 eV, respectively (Fig. 5(b)–(d)) and catalyst washcoat before and after the SRM reaction have the K-edge points at 8982.4, and 8982.15 eV, respectively (Fig. 5(a) and (e)). It is found that the K-edge points of all the samples are very close to the Cu(II). Compared with the standard Cu(II) the offset is 0.25 eV due to 1*s* to 3*d* transition [8]. Since Cu ions are not entirely surrounded by oxygen atoms and

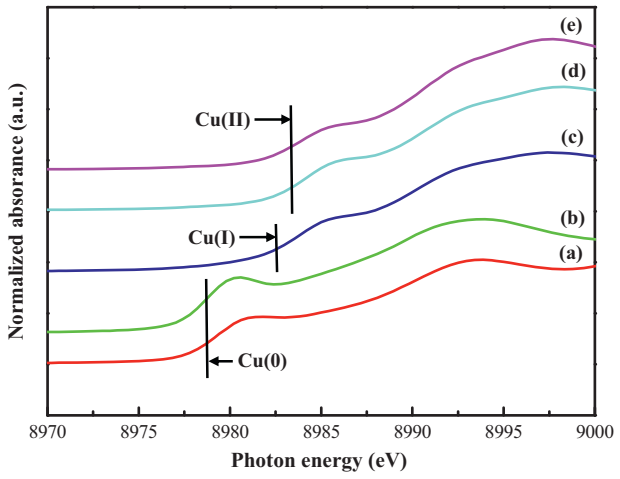

Fig. 5. XANES spectra of copper standards and copper species in the Cu/ZnO–Al_2O_3 catalyst with CeO_2 binder washcoats (S20-B2) (a) before reaction, (b) Cu foil, (c) Cu_2O, (d) CuO, and (e) after reaction for the steam reforming of methanol in a microreactor.

Table 3
Structural parameters of slurry (20 wt.% solid content with 2% CeO_2 binder solid at pH 7) before and after reaction analyzed by EXAFS.

Bonding pair	CN[a] (±0.05)	R[b] (Å) (±0.02 Å)	$\Delta\sigma^2$[c] ($Å^2$)
Fresh S20-B2 Cu–O	3.24	1.99	0.00398
Used S20-B2 Cu–O	10.22	1.95	0.00431

[a] CN: coordination number.
[b] R: bond distance.
[c] σ: Debye–Waller factor.

form oxides (OH^-) with the covalent bond, it gives slight shift. However, the well-defined shoulders at 8985.3 eV are attributed to the 1*s* to $4p_{xy}$ transition that indicates the existence of Cu(II) species in the washcoat slurries [8,28,29]. As prepared and after reaction, it has been evident from the XANES spectra that the observed samples can be ascribed the slight deflection of Cu(II) during the methanol reduction process in Fig. 5(e) and consisted with XRD analyses. To obtain the information on local structure around Cu(II) species in catalyst washcoat of the Cu/ZnO–Al_2O_3 catalysts with CeO_2 sols were analyzed with EXAFS spectra as shown in Table 3. Interestingly, the as-synthesized Cu/ZnO–Al_2O_3 catalysts with CeO_2 sols (S20-B2 sample before ATRM reaction) have consisted with the oxygen atom directly bonded to central Cu atom. It has the Cu–O bond length of 1.99 Å with the coordination number of 3.24. After the ATRM reaction, structures of the washcoat catalyst samples were transformed into copper oxide and the coordination number changed to 10.2 with a Cu–O bond distance of 1.95 Å. Two approaches were taken according with the fitting of the crystallographic data. In the first case, the coordination number was held at the crystallographic values with the radial distance and Debye–Waller factor were varied. Generally, according with the entire EXAFS data analyses of the Debye–Waller factors ($\Delta\sigma$) were less than 0.01 Å. The apparent shortening of the Cu–O bond length probably was caused by the random motion of surface atom on Cu particles instead of a true shortening of the bond distance. Thus is responsible for the low-temperature ATRM reaction and consistent with the XPS and XRD data analyses.

In addition, coordination and valance states of the paramagnetic Cu(II) species in the as-synthesized and after SRM reaction were also studied by EPR spectroscopy at room temperature as shown in Fig. 6. Since the minimum *g*-factor of the catalyst is 2.11 (g_{DPPH} factor = 2.0037 at 25 °C), it is likely that the Cu(II) species has a square-plane structure in as-synthesized CuO/ZnO–Al_2O_3 catalyst washcoats with CeO_2 sols slurry [30,31]. According with Fig. 6(a),

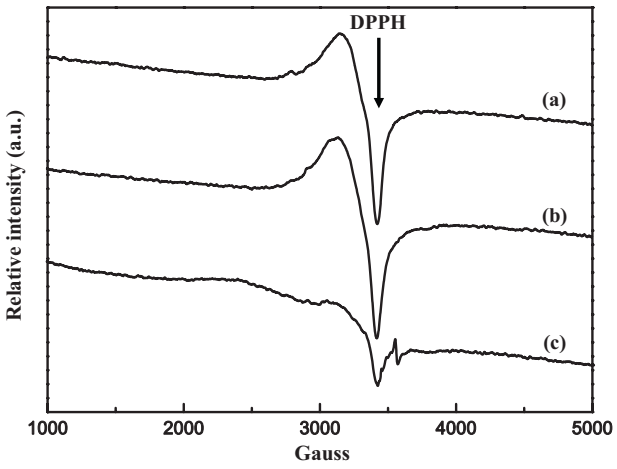

Fig. 6. EPR spectra of (a) fresh $Cu/ZnO–Al_2O_3$ catalyst, catalyst washcoat (S20-B2), (b) freshly prepared, and (c) after reaction measured at 300 K (ν_{EPR} = 9.784 GHz; Field (Gauss) = 3475 or g_{DPPH} = 2.0037; S20-B2 denotes "slurry of 20 wt.% solid content with 2 wt.% CeO_2 binder solid at pH 7").

the EPR spectrum of the fresh Cu catalyst at 25 °C is consisted with as-synthesized slurry. On the contrary, the spectrum (Fig. 6(c)) exhibits a dislocated broad signal. The spectrum is unlike that of any monomeric tetragonal copper (II) species. Furthermore, signal K at 3000 and 3568 G in the spectra corresponds to Cu(II)–Cu(II) ion pairs arising from the coupling between unpaired electrons of two Cu(II) ions [30,31]. This may suggests that the copper species may be interacted with ceria and consisted with the EXAFS/XANES and XRD analyses.

4. Conclusions

A significantly high active and stable $CuO/ZnO–Al_2O_3$ catalyst with CeO_2 sols washcoat catalyst was successfully investigated in a microchannel system for hydrogen generation integrated to a PEMFC system. The as-synthesized catalysts with the addition of CeO_2 sol were adversely affected the surface area and indicated high methanol conversations. According with the XRD patterns, catalyst sizes decrease with increasing CeO_2 sols. In addition, the XANES or EXAFS spectra identified the oxidative states and fine structures of the Cu species. A hydrogen production rate of 2.16 L h^{-1} was obtained at a feed rate of methanol liquid mixtures of 0.05–0.2 mL min^{-1} with a WHSV of 16.2 g_{MeOH} h^{-1} $g_{cat.}{}^{-1}$. Moreover, the methanol conversion was about 95% at 240 °C. This work showed that the feasibility of as-synthesized catalysts and the effects of CeO_2 binders for hydrogen production. With this approach, the feasible potential for production of high purity hydrogen can be achieved and final processing to make it suitable for an integrated PEMFC system.

References

[1] C. Horny, A. Renken, Catal. Today 120 (2007) 45–53.
[2] G. Germani, A. Stefanescu, Y. Schuurman, A.C.V. Veen, Chem. Eng. Sci. 62 (2007) 5084–5091.
[3] S. Patel, K.K. Pant, Appl. Catal. A: Gen. 356 (2009) 189–200.
[4] K. Geissler, E. Newson, F. Vogel, T.B. Truong, P. Hottinger, A. Wokaun, Phys. Chem. Chem. Phys. 3 (2001) 289–293.
[5] P.J.D. Wild, M.J.F.M. Verhaak, Catal. Today 60 (2000) 3–10.
[6] X. Yu, S.T. Tu, Z. Wang, Y. Qi, J. Power Sources 150 (2005) 57–66.
[7] T. Kim, D.H. Lee, D.E. Park, S. Kwon, ASME J. Fuel Cell Sci. Technol. 5 (1–6) (2008) 011008.
[8] C.G. Maciel, L.P.R. Profeti, E.M. Assaf, J.M. Assaf, J. Power Sources 196 (2011) 747–753.
[9] X. Yu, S.T. Tu, Z. Wang, Y. Qi, Chem. Eng. J. 116 (2006) 123–132.
[10] D.E. Park, T. Kim, S. Kwon, C.K. Kim, E. Yoon, Sens. Actuators A 135 (2007) 58–66.
[11] G.G. Park, S.D. Yim, Y. Yoon, W.Y. Lee, C.S. Kim, D.J. Seo, J. Power Sources 145 (2005) 702–706.
[12] A. Qi, B. Peppley, K. Karan, Fuel Process. Technol. 88 (2007) 3–22.
[13] M.S. Lim, M.R. Kim, J. Noh, S.I. Woo, J. Power Sources 140 (2005) 66–71.
[14] M.J. Stutz, D. Poulikakos, Chem. Eng. Sci. 63 (2008) 1761–1770.
[15] F.W. Lytle, J. Synchrotron Radiat. 6 (1999) 123–134.
[16] T. Resslert, J. Synchrotron Radiat. 5 (1998) 118–122.
[17] A.I. Nesvizhskii, J.J. Rehr, J. Synchrotron Radiat. 6 (1999) 315–316.
[18] S. Patel, K.K. Pant, Chem. Eng. Sci. 62 (2007) 5436–5443.
[19] C.S. Polster, H. Nair, C.D. Baertsch, J. Catal. 266 (2009) 308–319.
[20] Y. Liu, T. Hayakawa, K. Suzuki, S. Hamakawa, Catal. Commun. 2 (2001) 195–200.
[21] E. Moretti, M. Lenarda, L. Storaro, A. Talon, T. Montanari, G. Busca, E.R. Castellón, A.J. López, M. Turco, G. Bagnasco, R. Frattini, Appl. Catal. A: Gen. 335 (2008) 46–55.
[22] E. Moretti, M. Lenarda, L. Storaro, A. Talon, R. Frattini, S. Polizzi, E.R. Castellón, A.J. López, Appl. Catal. B: Environ. 72 (2007) 149–156.
[23] G. Avgoropoulos, T. Ioannides, Appl. Catal. A: Gen. 244 (2003) 155–167.
[24] N. Yi, R. Si, H. Saltsburg, M.F. Stephanopoulos, Energy Environ. Sci. 3 (2010) 831–837.
[25] G. Avgouropoulos, J. Papavasiliou, T. Ioannides, Chem. Eng. J. 154 (2009) 274–280.
[26] D.J. Seo, W.L. Yoon, Y.G. Yoon, S.H. Park, G.G. Park, C.S. Kim, Electrochim. Acta 50 (2004) 719–723.
[27] G. Huang, B.J. Liaw, C.J. Jhang, Y.Z. Chen, Appl. Catal. A 358 (2009) 7–12.
[28] S. Patel, K.K. Pant, J. Power Sources 159 (2006) 139–143.
[29] C. Lamberti, S. Bordiga, F. Bonino, C. Prestipino, G. Berlier, L. Capello, F. D'Acapito, F.X.L.I. Xamena, A. Zecchina, Phys. Chem. Chem. Phys. 5 (2003) 4502–4509.
[30] P. Bera, K.R. Priolkar, P.R. Sarode, M.S. Hegde, S. Emura, R. Kumashiro, N.P. Lalla, Chem. Mater. 14 (2002) 3591–3601.
[31] E.A. Aad, R. Bechara, J. Grimblot, A. Aboukais, Chem. Mater. 5 (1993) 793–797.